Biotechnology Frontiers
An International Journal
OPEN ACCESS
ISSN 3117-5791
Original Research article
Check for updates

Green Synthesis of Copper Oxide (CuO) Nanoparticles Using Tulsi (*Ocimum sanctum*) Leaf Extract: Structural Characterization, Antioxidant Activity and Antibacterial Activity against *Escherichia coli*

Pujatai A. Nawkhare

Department of Chemistry, Ambedkar College Arts Commerce and Science Chandrapur, 442401, India

Corresponding author: **Pujatai A. Nawkhare** | E-mail: **puja.nawkhare@gmail.com**

Citation: Pujatai A. Nawkhare (2026). Green Synthesis of Copper Oxide (CuO) Nanoparticles Using Tulsi (*Ocimum sanctum*) Leaf Extract: Structural Characterization, Antioxidant Activity and Antibacterial Activity against *Escherichia coli*. *Biotechnology Frontiers: An International Journal.* **DOI: https://doi.org/10.51470/BF.2026.6.2.16**

Received 12 July 2026 | Revised 09 August 2026 | Accepted 13 September 2026 | Available Online 14 October 2026

Abstract

Copper oxide (CuO) nanoparticles were prepared by an eco-friendly route using aqueous leaf extract of Tulsi (Ocimum sanctum) as a natural reducing and capping agent. X-ray diffraction (XRD) confirmed single-phase monoclinic CuO (tenorite, space group C2/c) with an average crystallite size of 33.0 nm from the Debye–Scherrer equation and 54 nm from the Williamson–Hall analysis, which also gave a lattice microstrain of 2.3×10^{-4}. Fourier-transform infrared (FTIR) spectroscopy showed Cu–O stretching bands at 603.75 and 512.12 cm^{-1} together with O–H, C=O, C–N and C–O bands of phytochemicals adsorbed on the particle surface. Scanning electron microscopy (SEM) revealed agglomerated, porous clusters of angular, faceted grains, and energy-dispersive X-ray (EDAX) analysis detected copper and oxygen as the principal elements, with adventitious carbon consistent with a residual organic capping layer. The nanoparticles showed concentration-dependent DPPH radical scavenging activity (89.45% at 1000 µg/mL; IC_{50} = 102.9 ± 0.02 µg/mL, against 19.97 ± 0.02 µg/mL for ascorbic acid). In the well-diffusion assay against Escherichia coli (MTCC 452), the nanoparticles produced a reproducible 12 mm zone of inhibition at every concentration tested (312.5–5000 µg/mL), compared with 30.5 mm for the ciprofloxacin control. These results show that Tulsi-mediated CuO nanoparticles combine antioxidant and antibacterial activity and merit further study, including determination of the minimum inhibitory concentration.

Keywords: *green synthesis; copper oxide nanoparticles; Ocimum sanctum (Tulsi); XRD; FTIR; SEM–EDAX; DPPH antioxidant activity; antibacterial activity; Escherichia coli.*

1. Introduction

Metal oxide nanoparticles have attracted wide interest because their small size and large surface-to-volume ratio give them optical, catalytic and biological properties that differ from those of the bulk material. Among them, copper oxide (CuO) is a p-type semiconductor with a narrow band gap, and it is inexpensive and relatively easy to prepare [1,2]. CuO nanoparticles have been explored for antimicrobial, antioxidant, catalytic and sensing applications [2,3]. Conventional physical and chemical routes to nanoparticles often need high energy input, toxic reagents or hazardous by-products. Green synthesis, in which plant extracts act as reducing and stabilizing agents, offers a simpler, cleaner and more economical alternative [2,4]. Plant extracts are rich in polyphenols, flavonoids, terpenoids, proteins and sugars, which can reduce metal ions and cap the growing particles, limiting uncontrolled growth and providing surface functional groups that may contribute to biological activity.

Tulsi (*Ocimum sanctum*, holy basil) is widely available in India and has a long history of use in traditional medicine. Its leaves contain phenolic compounds and flavonoids, which makes the extract a suitable candidate for nanoparticle synthesis [5]. Because resistant bacteria and oxidative stress-related disorders remain major health concerns, nanomaterials that show both antioxidant and antibacterial behaviour are of practical interest. *Escherichia coli* is a common Gram-negative test organism for such work. In this work, CuO nanoparticles were synthesized using Tulsi leaf extract and characterized by XRD, FTIR, SEM and EDAX. Their antioxidant activity was assessed by the DPPH radical scavenging assay, and their antibacterial activity against *E. coli* was evaluated by the agar well-diffusion method.

2. Materials and Methods

2.1 Preparation of Tulsi leaf extract

Fresh Tulsi (*Ocimum sanctum*) leaves were collected from local area, washed thoroughly with distilled water and dried.

© ***Authors:*** *Published in* ***Biotechnology Frontiers: An International Journal*** *under the CC BY-NC-ND 4.0 license (http://creativecommons.org/licenses/by-nc-nd/4.0/). No commercial use or modifications permitted.*

About 10 gm of leaves was boiled in 200 mL of distilled water at 40-50 °C for 2 hrs min, cooled and filtered through Whatman No. 1 filter paper. The filtrate was used as the reducing and capping agent.

2.2 Green synthesis of CuO nanoparticles

Copper precursor, e.g. copper sulphate pentahydrate merk was mixed with 640mL of Tulsi leaf extract under stirring at 50-60 °C] for 3 hrs min. a colour change was observed. The precipitate was collected by centrifugation, washed with distilled water and ethanol, dried at 80°C at oven and calcined at 400 °C for 3hrs to obtain CuO nanoparticles.

2.3 Characterization

The crystal structure was examined by powder XRD ,Cu Kα radiation, λ = 1.54059 Å) and compared with the reference tenorite CuO pattern (COD 9015822). The crystallite size (D) was calculated from the Debye–Scherrer equation:

$D = K\lambda / (\beta \cos\theta)$ (1)

where K = 0.9, λ is the X-ray wavelength, β is the full width at half maximum (FWHM) in radians and θ is the Bragg angle. To separate the contributions of crystallite size and lattice microstrain (ε) to peak broadening, the Williamson–Hall (uniform deformation model) relation was used:

$\beta \cos\theta = K\lambda / D + 4\varepsilon \sin\theta$ (2)

The dislocation density (δ) was estimated as:

$\delta = 1 / D^2$ (3)

Surface functional groups were identified by FTIR spectroscopy (Shimadzu) over 4000–400 cm^{-1} .The surface morphology was observed by SEM at ×250 and ×10,000 magnification, and the elemental composition and distribution were determined by EDAX elemental mapping and eZAF quantification.

2.4 Antioxidant activity (DPPH assay)

The free radical scavenging activity was determined by the DPPH (1,1-diphenyl-2-picrylhydrazyl) method [6,7]. In a 96-well plate, 10 µL of sample at different concentrations was added to 0.2 mL of 0.1 mM DPPH solution in methanol. Ascorbic acid was the positive standard (0–50 µg/mL), and the nanoparticles were tested over 0–1000 µg/mL. Reactions were run in quadruplicate with duplicate DPPH-free blanks. After 30 min of incubation in the dark, absorbance was read at 517 nm using a microplate reader (iMark, Bio-Rad). The percentage of radical scavenging activity (% RSA) was calculated as:

$\%\ RSA = [(Abs_control - Abs_sample) / Abs_control] \times 100$ (4)

and the IC_{50} values were calculated with GraphPad Prism 6.

2.5 Antibacterial activity (well-diffusion assay)

Antibacterial activity was evaluated against *Escherichia coli* (MTCC 452) by the agar well-diffusion (Kirby–Bauer) method [8]. Mueller–Hinton agar plates were inoculated with 100 µL of bacterial culture adjusted to 0.5 McFarland standard (~1.5 × 10^8 CFU/mL). Wells were loaded with 50 µL of nanoparticle suspension at 0, 312.5, 625, 1250, 2500 and 5000 µg/mL. One well on each plate received the solvent alone (DMSO, vehicle control) and one received ciprofloxacin (3 µg) as the positive control (PC). Plates were incubated at 37 °C for 24 h, and the clear zones were measured in mm. All nanoparticle plates were run in duplicate (Plate A and Plate B).

3. Results and Discussion

3.1 XRD analysis

The XRD pattern of the Tulsi-mediated CuO sample was compared with the reference tenorite pattern (COD 9015822; monoclinic, space group C2/c; a = 4.6776 Å, b = 3.4593 Å, c = 5.1264 Å, β = 98.965°). The strong reflections, the most intense of which were (11−1) at 35.18° and (111) at 38.41°, all indexed to monoclinic CuO (Table 1), and no reflections from Cu_2O, $Cu(OH)_2$ or unreacted precursor were detected. A very weak reflection at 30.18° (relative intensity 5.6) does not match any tenorite line. Given its low intensity it is most likely a trace impurity or residual phytochemical crystallite, and it could be checked against $Cu(OH)_2$ and basic copper carbonate references if full phase purity is to be claimed.

Table 1: XRD reflections of CuO–Tulsi nanoparticles, their indexing and Debye–Scherrer crystallite sizes

2θ (°)	d (Å)	(hkl)	Intensity	FWHM (°)	D (nm)
32.174	2.78	(110)	26.2	0.22	37.58
35.179	2.549	(11−1)	254	0.236	35.31
38.414	2.342	(111)	307	0.224	37.56
45.89	1.976	(11−2)	3.6	0.12	71.89*
48.416	1.879	(20−2)	68.7	0.248	35.12
53.14	1.722	(020)	18.8	0.273	32.54
57.97	1.59	(202)	39.3	0.27	33.64
61.232	1.513	(11−3)	48.2	0.219	42.15
65.475	1.424	(022)	42	0.27	34.98
65.992	1.415	(31−1)	43	0.23	41.18
67.8	1.381	(113)/(220)	57.5	0.42	22.79
72.14	1.308	(311)	27.5	0.36	27.30
74.963	1.266	(004)/(22−2)	30.1	0.5	20.02
79.91	1.2	(20−4)	5.6	0.33	31.40
82.32	1.17	(222)/(31−3)	27	1.34	7.87*
89.49	1.094	(13−1)/(131)	11	0.36	31.07

Excluded from the average: the 45.89° reflection is very weak (I = 3.6), giving an unreliably large size, and the 82.32° reflection has an anomalously broad FWHM (1.34°, 3–6 times that of neighbouring peaks), giving an unreliably small size. Average of the remaining 14 reflections: 33.0 nm

The average crystallite size from the Debye–Scherrer equation, using 14 reliable reflections, was about 33.0 nm (Fig. 1). The Williamson–Hall plot (Fig. 2) had a positive slope, indicating a small lattice microstrain of about 2.3 × 10^{-4}, and its intercept gave a crystallite size of about 54 nm. The dislocation density calculated from the Scherrer size was about 9.2 × 10^{14} lines/m^2. The difference between the two size estimates reflects the different assumptions of the methods, and it is therefore useful to report both values (Table 2).

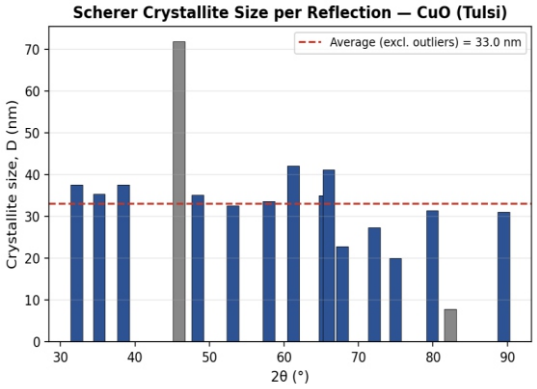

Fig. 1. Debye–Scherrer crystallite size for each XRD reflection of CuO–Tulsi. Grey bars mark the two excluded outliers.

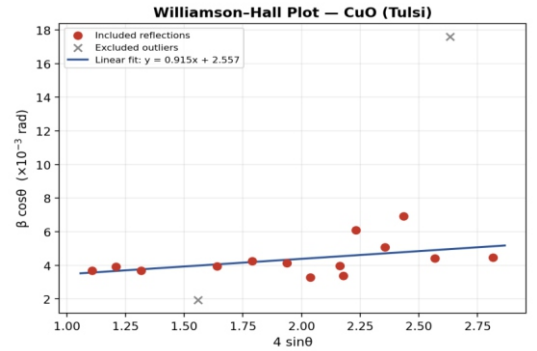

Fig. 2. Williamson–Hall plot (β cosθ versus 4 sinθ) with linear fit. The grey × marks the excluded 82.32° reflection.

Table 2: Structural parameters of CuO–Tulsi nanoparticles derived from XRD

Parameter	Value
Phase (reference)	Monoclinic CuO, tenorite (COD 9015822)
Space group	C2/c
Reference lattice parameters	a = 4.6776 Å, b = 3.4593 Å, c = 5.1264 Å, β = 98.965°
Average crystallite size, Debye–Scherrer	≈ 33.0 nm
Crystallite size, Williamson–Hall	≈ 54 nm
Lattice microstrain (ε)	≈ 2.3 × 10^{-4}
Dislocation density (δ)	≈ 9.2 × 10^{14} lines/m^2

3.2 FTIR analysis

The FTIR spectrum (Fig. 3, Table 3) was recorded to identify the functional groups on the nanoparticle surface and to confirm formation of the metal–oxygen lattice. The broad, intense band at 3367.86 cm^{-1} is assigned to O–H stretching of adsorbed water and of phenolic and hydroxyl groups from the Tulsi phytoconstituents (e.g. flavonoids, tannins). The weak bands at 3960.99 and 3843.33 cm^{-1} correspond to overtone/combination bands and free surface hydroxyl stretching, and the weak bands between 2423.66 and 2040.77 cm^{-1} are largely due to atmospheric CO_2 and combination modes. The band at 1627.99 cm^{-1} is assigned to C=O stretching (amide I) and/or aromatic C=C stretching, overlapping with the bending mode of adsorbed water. The bands at 1539.26 and 1390.74 cm^{-1} correspond to N–H bending/aromatic C=C stretching (amide II) and to C–N stretching/symmetric carboxylate (COO^-) stretching, respectively, indicating residual proteins and phenolic biomolecules acting as capping and stabilizing agents.

The bands at 1221.96 and 1072.47 cm^{-1} are attributed to C–O stretching of phenolic or ester groups and C–O–C stretching of polyol/polysaccharide constituents. The bands at 914.30 and 792.78 cm^{-1} are assigned to C–H out-of-plane bending and Cu–O–H bending vibrations. Most diagnostically, the pair of bands at 603.75 and 512.12 cm^{-1} is assigned to Cu–O stretching of the monoclinic CuO lattice. The presence of these low-wavenumber bands, with no bands attributable to unreacted copper precursor, supports formation of the CuO phase, in agreement with the XRD result, while the O–H, C=O, C–N and C–O bands confirm a biomolecule-derived organic layer on the particle surface.

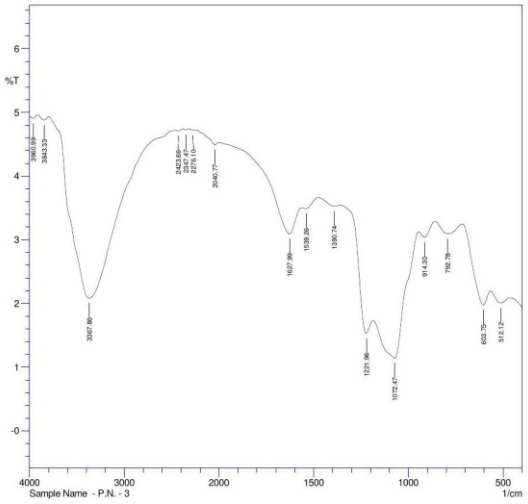

Fig. 3. FTIR spectrum of Tulsi-mediated CuO nanoparticles (4000–400 cm^{-1}).

Table 3: FTIR peak assignments for CuO–Tulsi nanoparticles

Peak (cm^{-1})	Intensity	Assignment
3960.99 / 3843.33	Weak, sharp	Overtone/combination bands; free surface O–H stretching
3367.86	Broad, strong	O–H stretching (adsorbed water; phenolic –OH of Tulsi phytoconstituents)
2423.66 / 2347.47 / 2276.10	Weak	Atmospheric CO_2 / combination bands
2040.77	Weak, broad	Combination band
1627.99	Medium	C=O stretching (amide I) / aromatic C=C; O–H bending of water
1539.26	Weak–medium	N–H bending / aromatic C=C stretching (amide II)
1390.74	Weak–medium	C–N stretching / symmetric COO^- stretching
1221.96	Weak	C–O stretching of phenolic/ester groups
1072.47	Medium	C–O–C stretching of polyols/polysaccharides
914.30 / 792.78	Weak–medium	C–H out-of-plane bending / Cu–O–H bending
603.75 / 512.12	Medium	Cu–O stretching, monoclinic CuO lattice

3.3 SEM and EDAX analysis

At low magnification (×250, Fig. 4a) the CuO–Tulsi sample appeared as highly agglomerated, porous clusters of irregular granular particles. Such agglomeration is common in plant-mediated synthesis, where capping biomolecules promote nucleation but also encourage secondary clustering during drying and calcination. At ×10,000 (Fig. 4b) the individual grains were angular and plate-like with sharp, well-defined edges, and fine particulates decorated the surfaces of the larger grains, suggesting nucleation of smaller CuO particles on larger secondary aggregates.

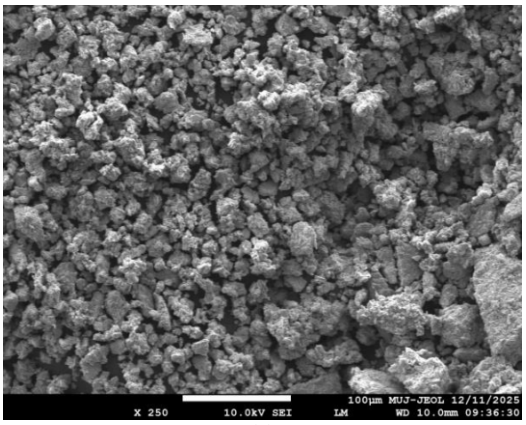

(a)

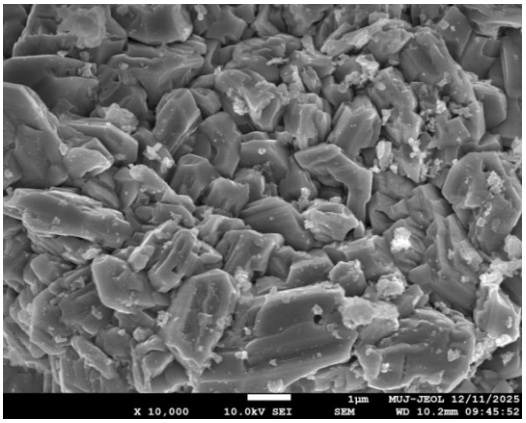

(b)

Fig. 4. SEM micrographs of Tulsi-mediated CuO nanoparticles at (a) ×250 (100 µm scale bar) and (b) ×10,000 (1 µm scale bar).

EDAX elemental mapping (Fig. 5) showed copper and oxygen distributed across the imaged region, with copper-rich domains corresponding to the denser clusters and oxygen distributed fairly uniformly. The sum spectrum (Fig. 6) contained two dominant peaks, O Kα and Cu Lα, with no peaks from other metallic contaminants. Quantification (Table 4, Fit A) gave 70.0 wt% Cu and 30.0 wt% O (37.0 at% Cu, 63.0 at% O). This is richer in oxygen than the ideal 1:1 Cu:O ratio of CuO (about 79.9 wt% Cu), which is often seen for green-synthesized oxides because oxygen-containing surface species (adsorbed water, hydroxyl and carboxylate groups of the capping layer) add to the oxygen signal and because EDAX is less accurate for light elements. The result therefore confirms a copper oxide with no foreign metals, and the CuO phase assignment rests mainly on the XRD and FTIR data.

When adventitious carbon was included in the fit (Table 4, Fit B), the composition was 24.9 at% Cu, 48.7 at% O and 26.4 at% C. The carbon is attributed to residual phytochemical capping agents (flavonoids, terpenoids, phenolics) from the Tulsi extract, in line with the FTIR results, although carbon tape or a conductive coating can also contribute to this signal [9].

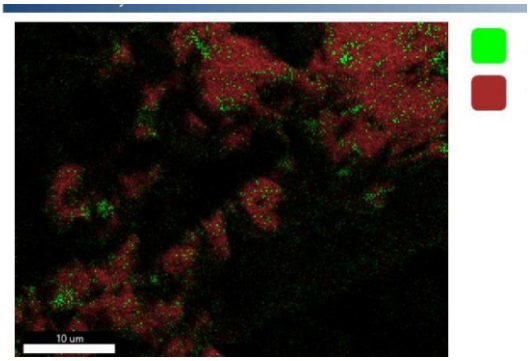

Fig. 5. EDAX elemental overlay map of the Live Map 1 region of interest showing O Kα (green) and Cu Lα (red).

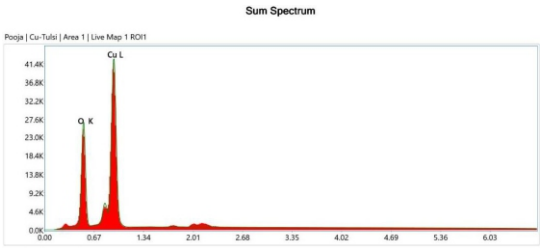

Fig. 6. EDAX sum spectrum of the CuO–Tulsi sample (Area 1, Live Map 1 ROI1) showing O Kα and Cu Lα peaks.

Table 4: eZAF quantification of the EDAX sum spectrum (analysis uncertainty 99.00%)

Element	Fit A: wt%	Fit A: at%	Fit B (with C): wt%	Fit B (with C): at%
C K	–	–	11.8	26.4
O K	30.0	63.0	29.1	48.7
Cu L	70.0	37.0	59.1	24.9

Errors (%): Fit A – O 7.4, Cu 7.0; Fit B – C 11.2, O 8.0, Cu 7.0.

3.4 Antioxidant activity

The DPPH radical scavenging activity of CuO–Tulsi increased with concentration, from 5.31% at 1 µg/mL to 89.45% at 1000 µg/mL, passing 50% between 100 µg/mL (48.66%) and 250 µg/mL (71.81%) (Table 5, Fig. 7a). Ascorbic acid, tested over the lower range of 0–50 µg/mL, reached 84.20% at 50 µg/mL (Fig. 7b). The IC_{50} of CuO–Tulsi was 102.9 ± 0.02 µg/mL compared with 19.97 ± 0.02 µg/mL for ascorbic acid, so the nanoparticles were about 5.15-fold less potent than the pure standard on a mass basis, which is expected for a purified antioxidant compound. The two series were measured over different concentration ranges, so percentage values at the same concentration should not be compared directly.

In a screen of nine metal oxide–plant combinations (FeO, NiO and CuO with Tulsi, Neem and Aloe vera extracts), CuO–Tulsi was one of only three samples for which an IC_{50} could be determined within 0–1000 µg/mL, the others being NiO–Neem (95.24 ± 0.02 µg/mL) and NiO–Tulsi (140.3 ± 0.02 µg/mL). The remaining six samples did not reach 50% scavenging in this range. The activity of CuO–Tulsi is likely due to residual phenolic and flavonoid compounds from the Tulsi extract adsorbed on the nanoparticle surface, which the FTIR and EDAX results support, although a contribution from the CuO itself cannot be ruled out. Antioxidant activity has also been reported for Cu and Ag nanoparticles prepared with *Ocimum sanctum* leaf extract [5].

Table 5: DPPH radical scavenging (% RSA) of CuO–Tulsi nanoparticles and ascorbic acid

CuO–Tulsi (µg/mL)	% RSA	Ascorbic acid (µg/mL)	% RSA
0	0.00	0	0.00
1	5.31	0.78125	0.85
10	9.96	1.5625	1.59
50	32.26	3.125	6.98
100	48.66	6.25	18.69
250	71.81	12.5	30.18
500	82.31	25	55.92
1000	89.45	50	84.20

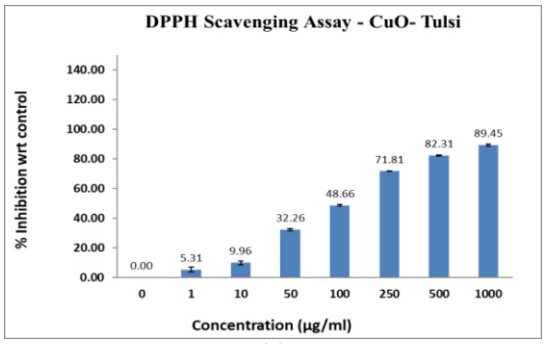

(a)

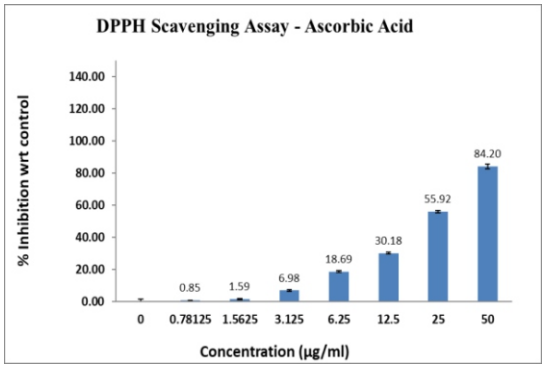

(b)

Fig. 7. DPPH radical scavenging (%) of (a) CuO–Tulsi nanoparticles (0–1000 µg/mL) and (b) ascorbic acid (0–50 µg/mL).

3.5 Antibacterial activity against E. coli

CuO–Tulsi produced clear zones of inhibition against *E. coli* (MTCC 452) at all concentrations tested (Table 6, Fig. 8). The zone was 12 mm at every concentration from 312.5 to 5000 µg/mL, with no variation between the duplicate plates, while the vehicle control (DMSO) produced no zone. The ciprofloxacin control (3 µg) gave a zone of 30.5 mm (SD 0.71). The unchanged zone size over a 16-fold concentration range suggests that the antibacterial effect saturates at or below the lowest concentration tested, probably because of limited diffusion of the nanoparticles through the agar. The minimum inhibitory concentration is therefore likely to lie below 312.5 µg/mL, and it should be determined by a broth microdilution method. MIC values of 62.5–125 µg/mL against *E. coli* have been reported for CuO nanoparticles made with neem and jojoba extracts [9,11,13], which is below the lowest concentration used here. Compared with the other copper oxide samples prepared with different plant extracts (Table 7), CuO–Tulsi was the only one to reach its full effect at the lowest concentration: CuO–Aloevera reached similar zones only at 625–1250 µg/mL, and CuO–Neem reached a comparable zone (13 mm) only at 5000 µg/mL.

The antibacterial action of copper oxide nanoparticles is commonly attributed to release of Cu^{2+} ions, generation of reactive oxygen species and damage to the cell membrane [3,9,12]; these mechanisms were not examined in the present work, and the role of the Tulsi capping layer remains to be studied.

Table 6: Zone of inhibition of CuO–Tulsi nanoparticles against E. coli (MTCC 452)

Concentration (µg/mL)	Plate A (mm)	Plate B (mm)	Mean (mm)	SD
Ciprofloxacin, 3 µg (PC)	31	30	30.5	0.71
0 (vehicle control)	0	0	0	0
312.5	12	12	12	0
625	12	12	12	0
1250	12	12	12	0
2500	12	12	12	0
5000	12	12	12	0

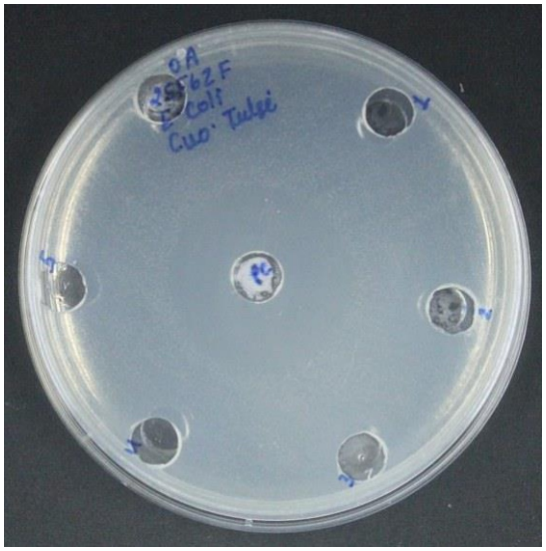

Plate A



Plate B

Fig. 8. Well-diffusion plates of CuO–Tulsi against E. coli, showing clear zones around the sample wells and around the central ciprofloxacin (PC) well.

Table 7. Zone of inhibition (mm) of CuO nanoparticles prepared with different plant extracts against E. coli.

Concentration (µg/mL)	CuO–Tulsi	CuO–Neem	CuO–Aloevera
312.5	12	4.33	8.33
625	12	4.33	12.33
1250	12	8.67	12.67
2500	12	8.67	13
5000	12	13	13.67

4. Conclusion

CuO nanoparticles were synthesized using Tulsi (*Ocimum sanctum*) leaf extract. XRD showed single-phase monoclinic CuO with a crystallite size of about 33 nm (Debye–Scherrer) or 54 nm (Williamson–Hall) and a small microstrain of 2.3×10^{-4}. FTIR confirmed Cu–O lattice vibrations and a capping layer of plant biomolecules[10]. SEM showed agglomerated, faceted particles, and EDAX confirmed copper and oxygen with residual carbon from the extract. The nanoparticles scavenged DPPH radicals in a concentration-dependent manner (IC_{50} = 102.9 ± 0.02 µg/mL) and produced a reproducible 12 mm inhibition zone against *E. coli* from 312.5 µg/mL upwards. These findings indicate that Tulsi-mediated CuO nanoparticles are a promising antioxidant and antibacterial material. Further work should determine the MIC and MBC, test Gram-positive organisms, examine the mechanism of action and assess cytotoxicity.

Conflict of Interest

The authors declare no conflict of interest.

References

1. Reddy, K. R. (2017). Green synthesis, morphological and optical studies of CuO nanoparticles. *Journal of Molecular Structure*, 1150, 553–557. https://doi.org/10.1016/j.molstruc.2017.09.005
2. Akintelu, S. A., Folorunso, A. S., Folorunso, F. A., & Oyebamiji, A. K. (2020). Green synthesis of copper oxide nanoparticles for biomedical application and environmental remediation. *Heliyon*, 6, e04508.
3. Letchumanan, D., Sok, S. P., Ibrahim, S., Nagoor, N. H., & Arshad, N. M. (2021). Plant-based biosynthesis of copper/copper oxide nanoparticles: an update on their applications in biomedicine, mechanisms, and toxicity. *Biomolecules*, 11(4), 564. https://doi.org/10.3390/biom11040564
4. Siddiqi, K. S., & Husen, A. (2020). Current status of plant metabolite-based fabrication of copper/copper oxide nanoparticles and their applications: a review. *Biomaterials Research*, 24(1), 11.
5. Ashokkumar, M., Palanisamy, K., Ganesh Kumar, A., Muthusamy, C., & Senthil Kumar, K. (2024). Green synthesis of silver and copper nanoparticles and their composites using *Ocimum sanctum* leaf extract displayed enhanced antibacterial, antioxidant and anticancer potentials. *Artificial Cells, Nanomedicine, and Biotechnology*, 52, 438–448. https://doi.org/10.1080/21691401.2024.2399938
6. Abdulrasheed-Adeleke, T., & Musa Bola, B. (2020). Comparative in vitro antioxidant activities of aqueous extracts of *Garcinia kola* and *Buchholzia coriacea* seeds. *Tanzania Journal of Science*, 46, 498–507.
7. Imam, M. Z., Akter, S., Hoque Mazumder, M. E., & Rana, S. (2011). Antioxidant activities of different parts of *Musa sapientum* L. ssp. *sylvestris* fruit. *Journal of Applied Pharmaceutical Science*, 1, 68–72.
8. Christenson, J. C., Korgenski, E. K., & Relich, R. F. (2018). Laboratory diagnosis of infection due to bacteria, fungi, parasites, and rickettsiae. In *Principles and Practice of Pediatric Infectious Diseases* (5th ed., pp. 1422–1434.e3). Elsevier.
9. Khairy, T., Amin, D. H., Salama, H. M., Elkholy, I. M. A., Elnakib, M., Gebreel, H. M., … Sayed, H. A. E. (2024). Antibacterial activity of green synthesized copper oxide nanoparticles against multidrug-resistant bacteria. *Scientific Reports*, 14, 25020. https://doi.org/10.1038/s41598-024-75147-0.
10. Alok Kumar Srivastava, Virendra Kishor Sangode, K. V. Shalini, and Sangeetha Shanmugam (2026). Modern Nano-Fertilizer Delivery Systems and Nano-Biofertilizers: Advances, Mechanisms, and Sustainable Applications in Climate-Smart Agriculture: A Comprehensive Review. *Journal of Diversity Studies*. DOI: https://doi.org/10.51470/JOD.2026.5.1.146.
11. Rohan Gavankar, Deepa Verma, Ankita S. Tekade, and Virendra Sangode (2026). Green Synthesis and Characterization of Zinc Oxide Nanoparticles Using *Cyperus pangorei* Grass Extract and its Antibacterial Activity. *Journal of Diversity Studies*. DOI: https://doi.org/10.51470/JOD.2026.5.1.195
12. Kamal Vatika, Lisha, Shamal Kumbhar, Mehtab Yasmeen, Sunil Akare and Virendra K. Sangode (2024) Nanoparticle of *Azadirachta indica* (Neem) mitigating lead acetate induced reproductiive toxicity. *Biochem. Cell. Arch.* 24, 1101-1109. DOI: https://doi.org/10.51470/bca.2024.24.1.1101
13. Chetankumar B Masram, Virendra K Sangode, Prakash Tanji Wankhedkar, Manish Dnyaneshwar Baviskar, and Ravindra Yadav Bhandare [2026]. Green Synthesis of Silver Nanoparticles Using *Murraya Koenigii*: Characterization, Antioxidant, and Antibioilm Potential. *Journal of Diversity Studies*. DOI: https://doi.org/10.51470/JOD.2026.5.1.339